AN EVALUATION OF METHODS AND ASSUMPTIONS USED IN POTENTIAL FLOW MODELLING OF SWIRL RECOVERY VANES

Barkın Sarıgöl

A thesis submitted in partial fulfillment of the requirements for
Bachelor of Aerospace Engineering Honours Programme

Faculty of Aerospace Engineering
Delft University of Technology
April 2023

TU Delft

AN EVALUATION OF METHODS AND ASSUMPTIONS USED IN POTENTIAL FLOW MODELLING OF SWIRL RECOVERY VANES

Barkın Sarıgöl
Delft University of Technology, Netherlands - April, 2023

Various potential flow methods with different assumptions are available to quantify the efficiency increase and thrust provided by a swirl recovery vane (SRV). In this paper, thrust coefficients and efficiency results obtained by different potential flow methods for the same SRV geometry at different advance ratios are presented. The methods include two VLM and four lifting line (LL) models with different assumptions. The models are compared in terms of accuracy with respect to RANS results and computational cost. This makes it possible to evaluate the benefits and drawbacks of neglecting or accounting for the presence of certain effects and modelling choices. The effects taken into account or deliberately neglected in different models include; finite propeller-SRV distance, nacelle presence, wake and free stream nonalignment, flow interaction between vane blades, the Kutta condition and SRV sweep. The wake angle behind the SRV is also varied and its effect on thrust coefficient is observed. In conclusion, accounting for the presence of a nacelle and finite slipstream distance respectively leads to 7.28% and 16.39% improvement in accuracy of the SRV thrust coefficient with negligible increase in CPU time. Not aligning the SRV wake with free stream direction has little impact on the computed thrust coefficient but causes the CPU time to increase steeply. Using a VLM based model rather a LL model and modelling vane interaction significantly increases CPU time whilst yielding the highest improvements in thrust coefficient accuracy (25.43% and 35.16%).

Nomenclature

C_{T_V} = SRV thrust coefficient [-]
$(V_{\Gamma_{jit}})$ = magnitude of the tangential component of the velocity induced by the jth Horseshoe vortex at the ith bound vortex [m/s]
α_{ind} = induced angle of attack [rad]
α_i = geometric angle of attack at ith location [rad]
$\alpha_{L=0}$ = 0 lift angle of attack [rad]
α_{rot} = local flow rotation due to finite SRV-propeller distance [rad]
η_P = isolated propeller efficiency [-]
η_{sys} = efficiency of SRV+propeller system [-]
Γ_i = circulation of at ith location [m^2/s]
ϕ = local swirl angle [rad]
ρ = air density [kg/m^3]
θ_i = local SRV angle w.r.t free-stream direction [rad]
$\vec{n}$ = local normal to SRV surface [rad]
$V_{\vec{ctrl}_{\Gamma_{ji}}}$ = total velocity at the ith control point [m/s]
$\vec{V_{\Gamma_{ji}}}$ = velocity induced by the jth Horseshoe vortex at the ith bound vortex [m/s]
$V_{\vec{bound}_i}$ = total velocity at the ith Horseshoe bound vortex [m/s]
$\vec{V_{ctrl_i}}$ = total velocity at the control (collocation) point associated with the ith Horseshoe [m/s]
a_0 = airfoil lift curve slope [1/°]
c = local SRV chord [m]
C_P = power coefficient [-]
C_{T_P} = thrust coefficient of only propeller [-]
D_P = propeller diameter [m]
dF_i = force created by the ith Horseshoe vortex

element [N]

dl = horseshoe bound vortex length [m]

J = propeller advance ratio [-]

n_s = propeller rotational frequency [s^{-1}]

r = spanwise distance between bound horseshoe vortex and propeller rotational axis [m]

R_n = nacelle radius [m]

r_{im} = spanwise distance between an image vortex and propeller rotational axis [m]

T_P = thrust of propeller [N]

T_V = thrust of the SRV [N]

u_∞ = unit vector along the free stream direction [-]

u_i = velocity induced by ith horseshoe vortex at propeller [m/s]

V_∞ = aircraft free stream velocity [m/s]

V_{a_i} = axial (free-stream direction) component of propeller slipstream velocity at the ith location [m/s]

V_{t_i} = tangential (azimuthal) component of propeller slipstream velocity at the ith location [m/s]

V_{in_i} = propeller slipstream velocity magnitude at the ith location [m/s]

d_h = distance between jth horseshoe vortex and ith location [m]

d = axial correction distance [m]

= unit vector in the free stream velocity direction [-]

I. INTRODUCTION

Engineers have come up with different methods to increase the efficiency of propeller propulsion systems. A simple method that can increase the propulsive efficiency of an aircraft is a swirl recovery vane (SRV). SRV is a stator that is used to increase the propulsion efficiency of a propeller system by converting the rotational energy in the propeller slipstream into additional thrust. The SRVs can already be seen in the next generation CFM RISE open fan engine concepts, making it important to understand their modelling.

During the design process of an SRV, an initial optimization needs to be performed before the use of CFD to save computational effort. However, the design procedure of the SRVs are not well developed [1]. A common method of modelling the SRV in the early design stage is through the use of lifting line (LL) theory. It was observed by Li that although the lifting line method predicted that the SRV would produce 3.4% of the thrust of the propeller, wind tunnel observations showed that the SRV only produced 2.6% [1]. This is a 30% error, which is significant especially given the fact that the efficiency gain from the SRV is already low (found to be of order 2% for a typical uninstalled tractor propeller configuration using RANS [2]). Thus, to be able to produce an effective SRV design, it is important to acknowledge and carefully pick the assumptions of the models used in the design process. This raises the question: "Which assumptions in SRV potential flow modelling lead to the most error and which of these assumptions can be eliminated without significantly increasing the computational effort?"

In this paper, the thrust coefficient and efficiency of the same SRV geometry at different advance ratios are computed using two different Vortex Lattice Methods (VLM) and four different LL models. Each model differs from another by taking into account an effect that a different model assumed was not present. The difference in results between the models quantifies the increase in accuracy that can be obtained by modelling a certain effect or flow phenomena. Comparing the CPU time of the different models represents the computational cost of removing an assumption or taking into account a certain effect.

The effects or phenomena that are investigated include:

- Finite propeller-SRV distance: Assuming that the SRV does not change the flow profile directly after the propeller, the finite distance between propeller and SRV leads to a change in the angle of attack at the location of the SRV.
- Nacelle presence: The presence of a nacelle can be modelled by replacing it with a number of Horseshoe vortices such that the nacelle wall is represented as a free slip wall. This alters the flow field at the SRV blade.
- Non-alignment of SRV wake with free-stream

direction: The swirl direction of the wake downstream of the SRV is unknown when running a potential flow simulation. Thus, by prescribing the wake swirl at different feasible angles and comparing the SRV thrust for these different cases reveals the maximum error that can be made by picking an arbitrary swirl angle for the wake.

- Flow interaction between vane blades: Modelling all SRV blades together and using the induced velocity of one blade to impose flow tangency at another blade rather than modelling the flow around an isolated vane blade makes it possible to compute the effect of assuming infinite unperturbed flow in the tangential (azimuthal) direction.
- The Kutta condition: Since VLM modelling explicitly enforces the flow tangency unlike LL, the difference in thrust coefficients can be used to evaluate this effect.
- SRV Blade sweep: Using the VLM model to compute the effect on thrust of an SRV geometry when its sweep is increased highlights the severity of the error that would be made by neglecting the sweep. The sweep has to be neglected automatically if an LL model is used.

II. SRV PERFORMANCE PARAMETERS

The total propeller and vane efficiency can be defined as the system efficiency [1]:

$$\eta_{sys} = \frac{J \cdot (C_{T_P} + C_{T_V})}{C_P} \tag{1}$$

The propeller thrust coefficient C_{T_P}, SRV thrust coefficient C_{T_V}, propeller advance ratio (J) and power coefficient C_P are defined as [1]:

$$C_{T_P} = \frac{T_P}{\rho \cdot {n_s}^2 \cdot {D_P}^4} \tag{2}$$

$$C_{T_V} = \frac{T_V}{\rho \cdot {n_s}^2 \cdot {D_P}^4} \tag{3}$$

$$J = \frac{V_\infty}{n_s \cdot D_P} \tag{4}$$

$$C_P = \frac{P}{\rho \cdot {n_s}^3 \cdot {D_P}^5} \tag{5}$$

Efficiency and the vane thrust coefficient are the main parameters that will be used to compare different models. By assuming that the upstream effect of the swirl recovery vane is small, it can be assumed that the power coefficient and the thrust coefficient of the propeller are unchanged by the addition of a swirl recovery vane. Indeed, this assumption is supported as the change in the power coefficient of the propeller after the addition of a swirl recovery vane remained in the range of 0% to 0.5% for advance ratios between 0.95 to 1.6 according to Stokkermans [3]. Also, the addition of the SRV led to a deviation between -0.1% to +0.3% in the thrust coefficient of the propeller.

III. MODELLED FLOW CONDITION

Given that the objective of this paper is to model the flow around a SRV system using various potential flow methods to quantify the effect of assumptions used in these models, the inflow conditions under which the simulations will be conducted must be clearly defined. The inflow conditions and the SRV geometry used in the simulations are taken from Stokkermans [3]. This is useful for the verification of the results as doing this allows for a comparison between the VLM and LL results produced in this paper and the already existing CFD results obtained by Stokkermans. The free stream velocity V_∞ is 68m/s. Propeller and SRV diameters both equal D_P =0.5m. Nacelle radius is 0.0625m. Fig. 1, Fig. 2 and Fig. 3 respectively present the local pitch angle of the modelled SRV, axial and tangential velocity at different propeller advance ratios.

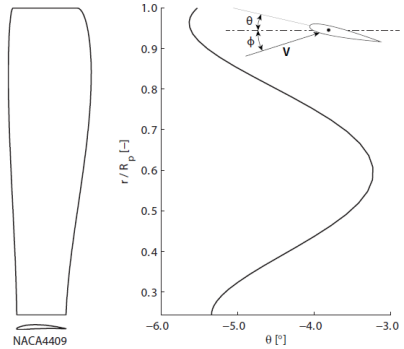

Figure 1. SRV local pitch angle and chord distribution as a function of radius [3]

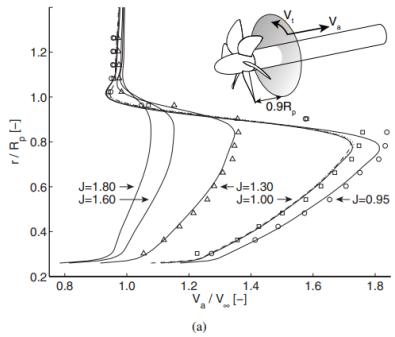

Figure 2. Axial inflow velocities at 0.9 propeller radii behind the propeller at different advance ratios [3]

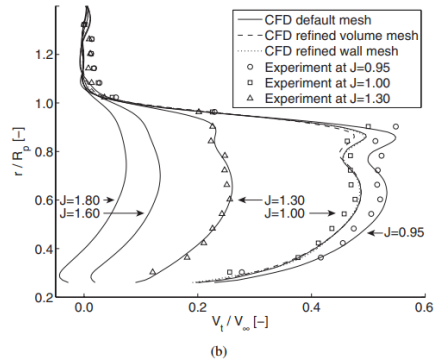

Figure 3. Tangential inflow velocities at 0.9 propeller radii behind the propeller at different advance ratios [3]

It is important to note that the contraction of stream tube behind the propeller is assumed to be negligible leading to the assumption that the radial velocity is zero.

The modelled SRV has 4 vanes, placed axis-symmetrically. The SRV is assumed to be two propeller radii behind the propeller as done in Stokkerman's CFD simulations. Lastly, in order to convert the thrust of the SRV into coefficients, some data about the isolated propeller must be known and is provided by Stokkermans for three advance ratios that will be used during the simulations with J=0.95 representing the high thrust take-off condition and J=1.6 representing the cruise condition:

Table 1. Isolated Propeller Quantities At Various Advance Ratios [3]

J	C_{T_P}	C_P	η_P
0.95	0.547	1.042	0.499
1.30	0.397	0.774	0.667
1.60	0.245	0.510	0.769

IV. POTENTIAL FLOW METHODS USED FOR MODELLING

The two main base models used are the VLM and the LL model. These base VLM and LL model are modified to generate two VLM and four different LL models. Although a VLM model has never before been used to model an SRV, it is possible in principle and is therefore evaluated in this paper.

A. Lifting Line for SRV Modelling

Using XFLR5, the 0-lift angle of attack and the lift curve slope for NACA4409 were found to be: -4.373 degrees and 0.1094 per degree respectively.

The fundamental equation of Prandtl's Lifting-Line theory at location i on an aircraft wing is given as [4]:

$$\frac{1}{4\pi V_\infty}\int_{-b/2}^{b/2}\frac{(d\Gamma/dy)dy}{y_i - y} + \alpha_{L=0_i} + \frac{2\Gamma_i}{V_\infty \cdot c_i \cdot a_0} = \alpha_i \quad (6)$$

The geometric angle of attack of the wing at location i (α_i) can be replaced with $\theta_i + \phi_i$ for an SRV. V_∞ may be replaced with the inflow SRV inflow speed V_{in_i}. The integral can be expressed as the sum of velocity induced by all the trailing vortices on the SRV blade to make the equation suitable for a numerical analysis. The modified lifting line theory at ith segment dl_i becomes:

$$\frac{-1}{V_{in_i}}\sum_{j=1}^{n}\left(-\frac{\Gamma_j}{4\pi(dl/2 + d_h)} + \frac{\Gamma_j}{4\pi(-dl/2 + d_h)}\right) + \alpha_{L=0} + \frac{2\Gamma_i}{V_{in_i}\cdot c_i \cdot a_0} = \theta_i + \phi_i \quad (7)$$

The distances d_h and dl can be seen in Fig. 4.

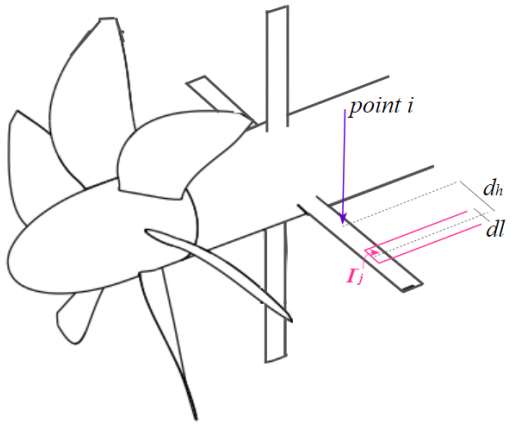

Figure 4. SRV Geometry (adapted from [3])

Where V_{in_i} is the incoming flow at the ith position and hence:

$$V_{in_i} = \sqrt{V_{t_i}^2 + V_{a_i}^2} \tag{8}$$

Then, the force in thrust direction on each element dl can be summed up to yield the resulting thrust on the SRV with 4 vanes [1]:

$$T_V = 4\rho \sum_{i=1}^{n} (V_{t_i} + \sum_{j=1}^{n} (V_{\Gamma_{ji}})_t) \cdot dl_i \cdot \Gamma_i \tag{9}$$

This model is the 'LL Base' model.

B. Accounting for Finite Slipstream Distance

An inherent limitation of the previous method was that the flow velocity V_{in} was assumed to be at an infinite distance away from the SRV. But in reality, this is not true and the SRV is at a finite distance from the propeller. An airfoil segment dl_i with circulation Γ_i in the SRV induces a flow velocity u_i at the location where the inflow conditions (shown in Figure 2 and Figure 3) are described [5]:

$$u_i = \frac{\Gamma_i}{2\pi d} = \frac{c_{l_i} \cdot c_i \cdot V_{in_i}}{4\pi d} = \frac{a_{0_i} \cdot (\alpha_i - \alpha_{L=0_i}) \cdot c_i \cdot V_{in_i}}{4\pi d} \tag{10}$$

But since the propeller slipstream velocity and direction is assumed to remain unaffected by adding the SRV, the flow at the SRV airfoil section must rotate by α_{rot} [5]:

$$\alpha_{rot} = \arctan \frac{u_i}{V_{in_i}} \approx \frac{u_i}{V_{in_i}} = \frac{a_{0_i} \cdot (\alpha_i - \alpha_{L=0_i}) \cdot c_i}{4\pi d} \tag{11}$$

This means that accounting for the interaction between the SRV and propeller in 3D flow yields:

$$\frac{c_l}{a_0} = \alpha - \alpha_{L=0} - \alpha_{ind} - \alpha_{rot} \tag{12}$$

This means that the fundamental equation of Prandtl's Lifting Line equation may be more correctly written as:

$$\frac{-1}{V_{in_i}} \sum_{j=1}^{n} \left(-\frac{\Gamma_j}{4\pi(dl/2 + d_h)} + \frac{\Gamma_j}{4\pi(-dl/2 + d_h)} \right) + \alpha_{L=0} + \frac{a_{0_i} \cdot (\theta_i + \phi_i - \alpha_{L=0_i}) \cdot c_i}{4\pi d} + \frac{2\Gamma_i}{V_{in_i} \cdot c_i \cdot a_0} = \theta_i + \phi_i \tag{13}$$

The term *'d'* in the modified Lifting Line equation must match the conditions used by Stokkermans. Stokkermans reported the velocity distributions at at 0.9 propeller radii behind the propeller and placed the SRV two propeller radii behind the propeller. Thus, the distance *'d'* is 1.1 propeller radii. This correction leads to the model 'LL w. Finite Slipstream Correction'. And the difference between C_{Tv} and efficiency computed using this model and the 'LL Base Model' highlights the magnitude of the improvement in accuracy when this effect is taken into account.

C. Modelling The SRV Nacelle

Another interesting factor to analyze is the presence of the nacelle in the flow. Different authors such as Stokkermans and Veldhuis have chosen to account for the presence of the nacelle whilst others such as Li have chosen not to include it in the modelling of the flow. Should the nacelle be modelled, it can be done so by placing an image vortex that corresponds to each Horseshoe vortex in the vane. In order to ensure that the flow component normal to the nacelle is equal to 0, the position of the ith image vortex is given by [6]:

$$r_{im} = \frac{R_n^2}{r} \tag{14}$$

Where r represents the position of the Horseshoe vortex on the vane with respect to the centre of the propeller rotation axis. This leads to the model 'LL with Nacelle Correction'. The results produced by

this model in comparison to the 'LL Base' model highlight the improvement in accuracy obtained by modelling the nacelle.

D. Wake Model Investigation

In all the previous lifting line models, the trailing horseshoe vortices and hence, the SRV wake was aligned with the free stream flow. But this could only happen when the tangential component of the flow is completely eliminated, implying complete swirl recovery. It is important to note that aligning the SRV wake with the free stream direction as if all swirl is eliminated does not lead to complete swirl recovery.

The other limiting case for the wake is if the wake is completely aligned with the propeller slipstream swirl direction (ϕ_i) which would happen if the SRV recovered no swirl from the flow. Again, it is important to emphasize that giving the trailing horseshoe vortices an angle of ϕ_i does not automatically lead to the no swirl recovery condition.

While conducting the LL simulation, the percentage of swirl recovery is unknown and hence, the correct angle of the wake cannot be deduced beforehand. However, the impact of this error on the vane thrust coefficient can be understood by simulating the SRV with trailing horseshoe vortex angles varying from 0 degrees (aligned with free stream direction) up to ϕ_i (aligned with propeller slipstream). Thus, aligning the wake with the free stream can be justified if the angle of the horseshoe vortices make an insignificant impact on the vane thrust coefficient. To simulate the angled wake conditions, the lifting line equation has to be modified. When the trailing horseshoe vortices at each location i is aligned with the local incoming flow (V_{ini}), the new lifting line equation at location i becomes:

$$\alpha_{L=0} + \frac{2\Gamma_i}{V_{ini} \cdot c_i \cdot a_0} = \theta_i + \phi_i + \arctan\left(\frac{\sum_{j=1}^{n} (V_{\Gamma_j})_t \cdot \cos(\phi_i) - (V_{\Gamma_j})_a \cdot \sin(\phi_i)}{V_{ini} + \sum_{j=1}^{n} (V_{\Gamma_j})_a \cdot \cos(\phi_i) + (V_{\Gamma_j})_t \cdot \sin(\phi_i)}\right) \tag{15}$$

The subscript t is used to indicate the tangential (azimuthal) component of induced velocity and a is used to indicate the axial (free-stream direction) of the induced velocity. This leads to the model 'LL w. Local Flow Oriented Trailing Vortices'. Comparing the results of this model to that of 'LL Base' model is effectively a comparison between the conditions where the horseshoe vortex directions are at their most extreme.

E. VLM for SRV Modelling

If each vane is divided into Horseshoe vortices with width dl, then the total aerodynamic force on the ith vortex is given by [7]:

$$\vec{dF_i} = \rho \Gamma_i \vec{V_{bound_i}} \times \vec{dl_i} \tag{16}$$

The total thrust created by the vanes can be expressed as the sum of axial component of force on each Horseshoe vortex:

$$T_V = (\sum_{i=1}^{n} \vec{dF_i})_a \tag{17}$$

At each bound vortex location i, the total velocity vector ($\vec{V_{bound_i}}$) can be expressed as a sum of the axial velocity and tangential velocity of the propeller slipstream and the velocity induced by all 'n' Horseshoe vortices at the bound part of the ith Horseshoe vortex. So the total velocity at the location of the ith Horseshoe bound vortex can be expressed as:

$$\vec{V_{bound_i}} = \vec{V_{a_i}} + \vec{V_{t_i}} + \sum_{j=1}^{n} \vec{V_{\Gamma_{ji}}} \tag{18}$$

It is known that the induced velocity by a Horseshoe vortex can be defined as shown in Equation 19, in accordance with Fig. 5 [8] where $\vec{dl_j}$ represents the bound vortex segment, $\vec{r_1}$ and $\vec{r_2}$ represent the vectors from the ends of $\vec{dl_j}$ going to the arbitrary point in space about which the induced velocity is evaluated, the double headed arrows represent the orientation of the jth circulation and u_∞ is the unit vector along the free stream velocity direction with which the trailing Horseshoe vortices are aligned:

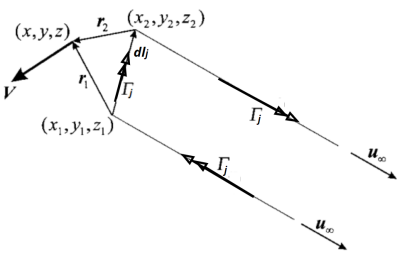

Figure 5. Vectors defining induced velocity (adapted from [7])

$$\vec{V_{\Gamma_{ji}}} = \Gamma_j \cdot c_{ji} \tag{19}$$

Given that this arbitrary point in space is the location of the ith Horseshoe's bound vortex, $\vec{r_1}$ and $\vec{r_2}$ can be rewritten as $\vec{r_{j_1 i}}$ and $\vec{r_{j_2 i}}$ [7].

$$c_{ji} = \frac{1}{4\pi}\left[\begin{array}{c} \frac{\vec{u}_\infty \times \vec{r}_{j_2 i}}{r_{j_2 i}\left(r_{j_2 i} - \vec{u}_\infty \cdot \vec{r}_{j_2 i}\right)} \\ + \frac{\left(r_{j_1 i} + r_{j_2 i}\right)\left(\vec{r}_{j_1 i} \times \vec{r}_{j_2 i}\right)}{r_{j_1 i} r_{j_2 i}\left(r_{j_1 i} r_{j_2 i} + \vec{r}_{j_1 i} \cdot \vec{r}_{j_2 i}\right)} \\ - \frac{\vec{u}_\infty \times \vec{r}_{j_1 i}}{r_{j_1 i}\left(r_{j_1 i} - \vec{u}_\infty \cdot \vec{r}_{j_1 i}\right)} \end{array}\right], \quad i \neq j$$

$$\mathrm{c}_{ji} = \tfrac{1}{4\pi}\left[\begin{array}{c} \frac{\vec{u}_\infty \times \vec{r}_{j_2 i}}{r_{j_2 i}\left(r_{j_2 i} - \vec{u}_\infty \cdot \vec{r}_{j_2 i}\right)} \\ - \frac{\vec{u}_\infty \times \vec{r}_{j_1 i}}{r_{j_1 i}\left(r_{j_1 i} - \vec{u}_\infty \cdot \vec{r}_{j_1 i}\right)} \end{array}\right], \quad i = j \tag{20}$$

The c_{ji} exception for when i=j is because the bound vortex of the jth Horseshoe does not induce velocity on itself. Finally, the circulations Γ_j need to be defined. This can be done by enforcing tangency to the surface of the swirl recovery vane at each of the control points associated with each jth Horseshoe vortex as conventionally done in VLM:

$$\vec{V_{ctrl_i}} \cdot \vec{n_i} = 0 \tag{21}$$

$$\vec{V_{ctrl_i}} = \vec{V_{a_i}} + \vec{V_{t_i}} + \sum_{j=1}^{n} \vec{V_{ctrl_{\Gamma_{ji}}}} \tag{22}$$

$$\vec{V_{ctrl_{\Gamma_{ji}}}} = \frac{\Gamma_j}{4\pi} \cdot \left[\begin{array}{c} \frac{\vec{u}_\infty \times \vec{r}_{j_2 i}}{r_{j_2 i}\left(r_{j_2 i} - \vec{u}_\infty \cdot \vec{r}_{j_2 i}\right)} \\ + \frac{\left(r_{j_1 i} + r_{j_2 i}\right)\left(\vec{r}_{j_1 i} \times \vec{r}_{j_2 i}\right)}{r_{j_1 i} r_{j_2 i}\left(r_{j_1 i} r_{j_2 i} + \vec{r}_{j_1 i} \cdot \vec{r}_{j_2 i}\right)} \\ - \frac{\vec{u}_\infty \times \vec{r}_{j_1 i}}{r_{j_1 i}\left(r_{j_1 i} - \vec{u}_\infty \cdot \vec{r}_{j_1 i}\right)} \end{array}\right] \tag{23}$$

In Eq. 23, $\vec{r_{j_1 i}}$ and $\vec{r_{j_2 i}}$ represent the vectors going from each end of $\vec{dl}_j$ to the ith collocation point.

Of course, this VLM method can be applied in multiple ways. The modelled SRV has four vanes. A method of modelling SRV can be simply placing one of the four vane blades in the flow to obtain the force created by that vane and then multiplying its thrust by four leading to the 'VLM Base Model'. This is similar to the approach used by Li [1]. But of course, this means that the aerodynamic interaction between the four vane blades is not taken into account and hence introduces the assumption of having infinite undisturbed flow in the tangential direction. This assumption can be removed by modelling all four of the vanes together to take this interaction into account. This involves using the velocity induced by the horseshoe vortices of one blade in the tangency equations (Equation (21)) of another blade leading to the model: 'VLM w. Vane Interaction'. The difference in C_{Tv} and efficiency produced by these two models speaks to the impact of neglecting the interaction between vane blades.

F. Comparison VLM and LL Modelling

The VLM and LL differ from one another in two main ways. Firstly, unlike the LL models, the VLM model can take into account SRV sweep. To test the impact of neglecting sweep, the SRV geometry described in Section III is changed by only modifying the leading edge sweep while keeping all other geometry parameters the same and the VLM base model is run at different sweep angles. Secondly, the other difference between the 'LL Base Model' and the 'VLM Base model' is that the VLM Base Model enforces tangency at all points and hence, the Kutta condition. Both in VLM and LL models (except the 'LL w. Local Flow Oriented Trailing Vortices' model), the wake has been aligned with the free stream velocity. The Kutta condition helps partially correct for this arbitrary choice at the vicinity of the airfoil trailing edge. Regardless of the arbitrary orientation of the trailing vortices, the magnitudes of the Horseshoe vortices adjust to enforce the Kutta condition as long as a collocation point is placed at the trailing edge. Thus, the difference between the 'LL Base Model' and the 'VLM Base model' results speaks to the magnitude of this correction.

V. Results & Discussion

The different variations of the VLM and LL model can be evaluated in terms of their accuracy with respect to the CFD results and their computational cost. Unless explicitly stated otherwise, for the lifting line models, a discretization of 40 Horseshoe vortices is used. For VLM models, 1600 Horseshoe vortices are used per vane blade (40 along span, 40 along chord).

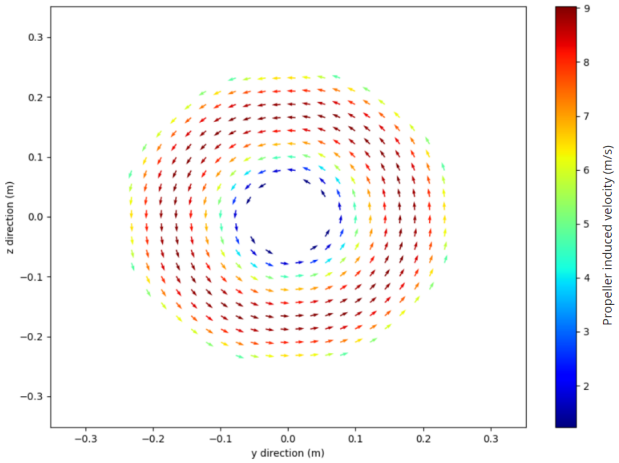

Figure 6. Propeller induced velocities at J=1.6 behind the propeller

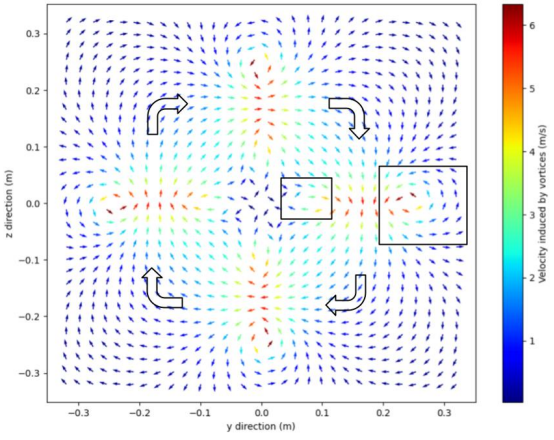

Figure 7. SRV induced radial and tangential velocities 0.5m behind the SRV leading edge at J=1.6 based on the 'VLM w. Vane Interaction' Model

Fig. 6 shows the flow velocities created by the propeller 0.5m behind the SRV leading edge.

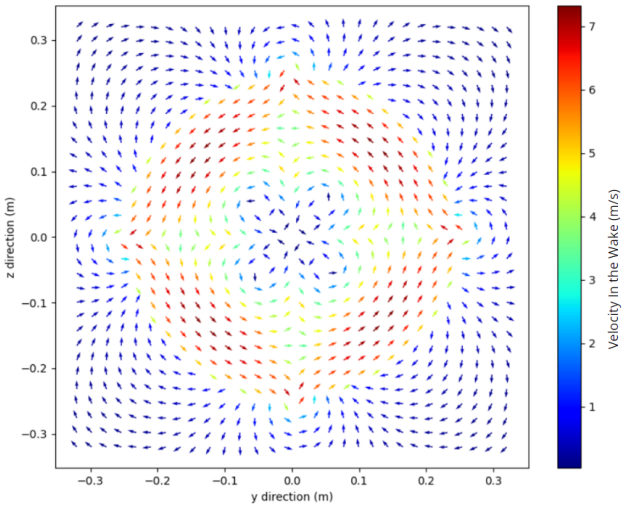

Figure 8. The complete flow 0.5m behind the SRV leading edge at J=1.6 (sum of propeller and SRV induced velocities)

The radial and tangential flow 0.5m downstream of the SRV leading edge is visualized in Fig. 7. The velocities are only due to the bound and trailing vortices of the SRV. The propeller induced velocities have been omitted for clarity sake. Fig. 8 shows the overall flow behind the SRV by superposing the propeller slipstream and SRV horseshoe-induced velocities.

It is possible to see that the SRV blades cause a downwash leading to an overall clockwise rotation, shown by the black arrows in Fig. 7. This rotation is in the opposite direction to that created by the propeller. In Fig. 7, although the majority of the flow is in the clockwise direction, the local tip vortices, one of which is highlighted in the larger black box in Fig. 7 cause local rotations in the counterclockwise direction. In addition, there are also tip vortices at the centre of the vane, shown inside the smaller black box in Fig. 7. This is because the nacelle that joins the SRV blades is not modelled by the 'VLM w. Vane Interaction' model. Superposing these velocities with that of the propeller leads to a reduction in the swirl indicating swirl recovery and lower swirl velocities as seen in Fig. 8 when compared to Fig. 6.

While developing the models, the upstream effect of the SRV on the propeller was neglected. In Fig. 9, the difference between the two RANS results highlights the impact of this assumption. The difference between the two results is negligible at advance ratios of 0.95 and 1.6, hence during the most significant portion of the flight.

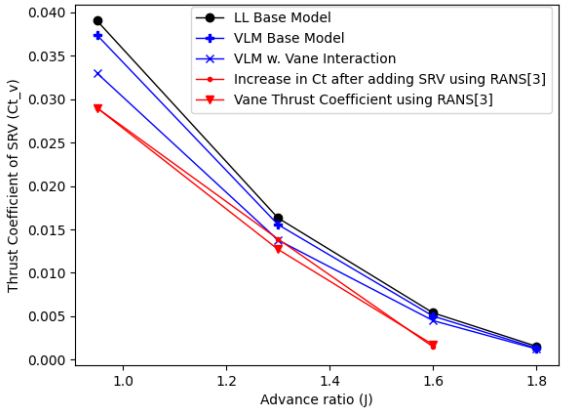

Figure 9. Vane thrust coefficient prediction of different models at various advance ratios

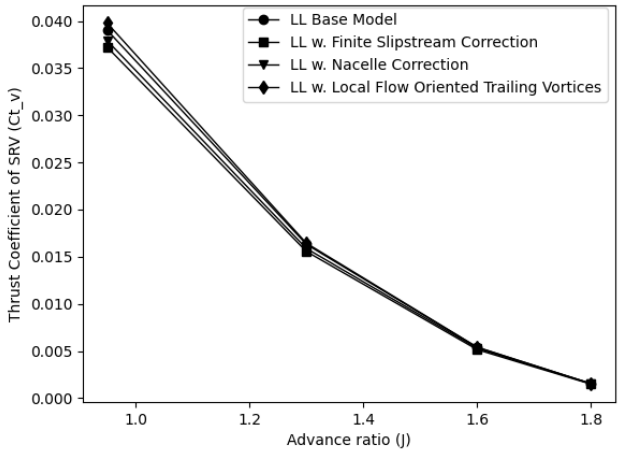

Figure 10. Vane thrust coefficient prediction of lifting line models

From Fig. 9, it can be seen that the difference between the potential flow methods and the RANS results become more pronounced at lower advance ratios and diverge. This is due to the increase of inflow (swirl) angle leading to increased parasitic drag. Another observation from Fig. 9 and Fig. 10 is that all VLM and LL models converge at very high advance ratios (J=1.8 and above) due to the reduction of the magnitude of the horseshoe vortices. Because of this, all the models have very similar cross-over advance ratios (advance ratio at which C_{T_v} becomes zero) as seen in Table 2.

Table 2. Model Cross-over Advance Ratio and CPU Time

Modelled Effect	**Cross Over J**	**CPU Time (s)**
LL Base Model	1.879	0.016
LL w. Finite Slipstream	1.881	0.016
LL w. Nacelle Correction	1.882	0.016
LL w. Local Flow Oriented Trailing Vortices	1.879	0.641
VLM Base Model	1.872	133.891
VLM w. Vane Interaction	1.876	257.403

Percentage improvement in the accuracy of the thrust coefficient computation due to each additional modelled effect is calculated using (24) and is tabulated in Table 3.

$$\left| \frac{C_{Tv}|_{w/o.assumption} - C_{Tv}|_{w.assumption}}{C_{Tv}|_{CFD}} \right| \cdot 100 \quad (24)$$

Table 3. Percentage Improvement of Potential Flow Modelling At Different Advance Ratios Due to Additional Modelled Effects

Modelled Effect	**J=1.3**	**J=1.6**
Finite Propeller-SRV Distance	5.45	16.39
Nacelle Hub Presence	3.15	7.28
Kutta Condition	5.46	25.43
Vane Interaction	12.78	35.16

From Table 3, it can be inferred that the second most significant improvement is obtained by modelling the Kutta condition. Unfortunately, this improvement leads to the most significant computational cost increase as seen in Table 2 by

comparing the CPU times of the 'LL Base Model' and 'VLM Base Model'.

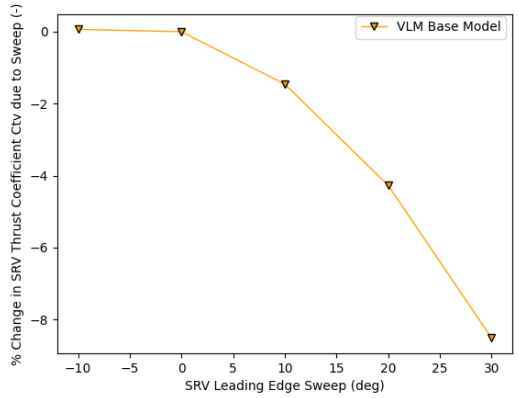

Figure 11. The change in vane thrust coefficient due to SRV sweep

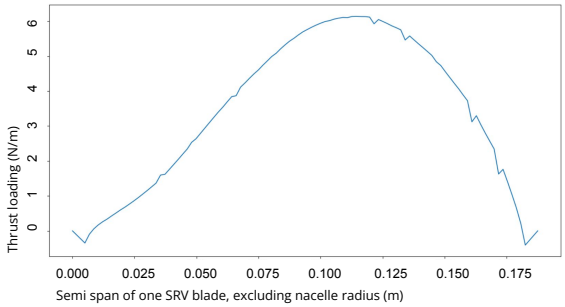

(a) No leading edge sweep

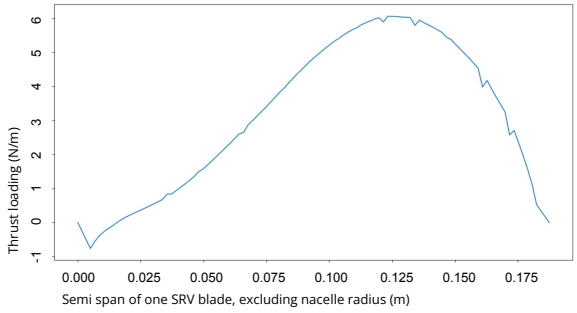

(b) +30 degree leading edge sweep

Figure 12. Thrust loading based on the 'VLM Base Model' with 10,000 horseshoe vortices at J=1.6

Another reason to use VLM instead of LL might be to take the sweep of the SRV into account. As seen in Fig. 11, this might be important at leading edge sweep angles of 20 degrees and above which might make using VLM worth the computational effort.

The reason for drop in the thrust coefficient at higher sweep angles can be seen by comparing Fig. 12a and Fig. 12b. When the sweep is increased, it is observed that at lower radial positions (near the centre of the SRV), less thrust is produced and more thrust is produced near the tip of the SRV. The first effect outweighs the second leading to a lower thrust coefficient.

The most significant improvement in accuracy is obtained by taking into account the aerodynamic interaction between individual SRV blades as seen in Table 3. However, this leads to a significant increase in the computation effort. According to Table 2, the CPU time is increased from 133.891 to 257.403 seconds. Most of the computational effort in the VLM is spent on using the Biot-Savart law to compute velocity induced by each horseshoe vortex at each collocation point and to solve the linear system. Since the vane blades are axis-symmetric, modelling four vane blades together instead of one blade does not quadruple the amount of unknown horseshoe vortices. The number of unknown horseshoe vortices to be solved remains the same meaning the CPU time of the solver does not increase. However, if there are 1600 horseshoe vortices and 1600 collocation points on one vane, the Biot-Savart law would have to be used $1600^2 = 2560000$ times to compute the velocity induced by 1600 horseshoe vortices at 1600 collocation points. When four blades are modelled, the Biot-Savart law has to be used $(4 \cdot 1600)^2 = 40960000$ times which is the reason for the steep increase in the CPU time.

Modelling the finite SRV-propeller distance and presence of the nacelle hub as a free-slip boundary leads to a small improvement in accuracy as seen in Table 3. However, comparing the CPU times of the 'LL Base Model', 'LL w. Finite Slipstream' and 'LL w. Nacelle Correction' in Table 2 shows that modelling these effects leads to no increase in the computational effort. Hence, it is always favorable

to model these effects.

Lastly, in order to put a cap on the error that could be made due to the trailing horseshoe vortices' direction being unknown, their direction was varied between 0 and ϕ_i degrees. The vane thrust coefficient was plotted for this range of angles in Fig. 13. The x-axis represents the angle of the wake as a fraction of ϕ_i.

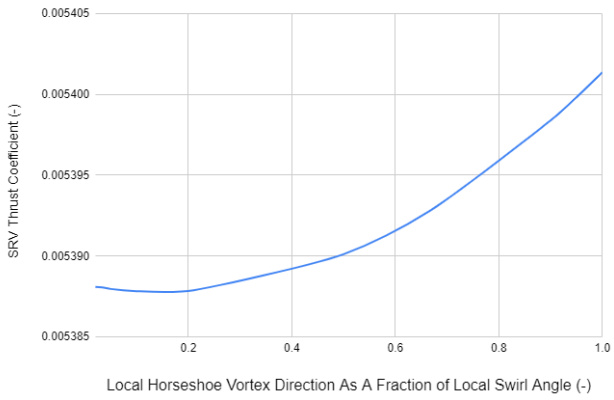

Figure 13. SRV Thrust Coefficient As A Function of Wake Angle at J=1.6

From 13, the difference between the maximum thrust coefficient and the minimum thrust coefficient is 0.25% meaning that the angle chosen for the wake has nearly no consequence on the vane thrust coefficient. However, not aligning the horseshoe vortices with the free-stream direction leads to more complex non-linear equations which have to be solved using an iterative solver. This results in an increased computational cost. The increase in CPU time can be seen by comparing 'LL Base Model' with 'LL w. Local Flow Oriented Trailing Vortices' in Table 2. This means that it is generally worth aligning the wake with the free stream direction as if the SRV completely recovers the swirl.

The larger picture can be analyzed by looking at the improvement in the thrust coefficient and efficiency of the propeller and SRV system as a whole, provided in Fig. 14. Regardless of the model used, the SRV is shown to lead to a distinct improvement in the thrust coefficient up to and including J=1.6. At J=1.6, even where the thrust coefficient predictions of different models seem to converge, the 'LL Base Model' predicts an increase of 2.20% in the thrust coefficient while RANS predicts 0.6% compared to the isolated propeller. This discrepancy once again highlights the importance of evaluating model assumptions.

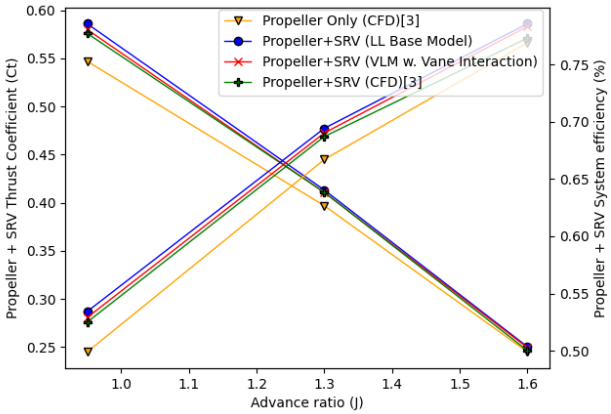

Figure 14. Thrust coefficient and system efficiency of the propulsion system without SRV and with SRV according to different models

VI. Conclusions

1) Based on vane thrust coefficient accuracy and computational cost criteria, it is nearly always favorable to model the fact that the SRV-propeller distance is finite and that there is a nacelle (as a free-slip wall) because the accuracy can be improved without increasing computational effort.
2) The alignment of the horseshoe vortices is arbitrarily chosen as the actual amount of swirl recovery is unknown. However, the maximum inaccuracy that can be caused by this is approximately 0.25%. Thus, it makes sense to align the trailing vortices with the axial direction to have linear equations and speed up the computation.
3) Using VLM instead of LL is beneficial in two ways: The Kutta condition on the SRV is modelled and the sweep of the SRV can be taken into account. Due to both these effects, using VLM leads to a significant improvement in the accuracy of the vane thrust coefficient despite coming at a significant computational

cost. However, this might be needed nevertheless when leading edge sweep of the SRV exceeds 20 degrees. A similar trade-off between computational effort and accuracy has to be made when deciding whether to model the interaction between different vane blades.

Acknowledgments

I would like to thank Prof. Dr. Ing. Georg Eitelberg for his guidance and encouragement. This paper would not be possible without his insight and experience. In addition, I would like to thank my father Tolga Hakkı Sarıgöl, also an aeronautical engineer for inspiring me to pursue this wondrous field.

References

[1] Li, Q., "Towards optimum swirl recovery for propeller propulsion systems," Ph.D. Thesis, Delft University of Technology, 2019.

[2] G. Eitelberg, T. S. T. S., L. Veldhuis, "ANALYSIS OF SWIRL RECOVERY VANES FOR INCREASED PROPULSIVE EFFICIENCY IN TRACTOR PROPELLER AIRCRAFT," *30th Congress of the International Congress of Aeronautical Sciences,*, 2016.

[3] T. Stokkermans, L. V., N. v. Arnhem, "Mitigation of propeller kinetic energy losses with boundary layer ingestion and swirl recovery vanes," *Royal Aeronautical Society Applied Aerodynamics Conference*, 2016.

[4] Anderson, J., *Fundamentals of Aerodynamics*, 6th ed., McGrawHill Education, 2017.

[5] Eitelberg, G., Pelt, T., Sinnige, T., and Raijmakers, E., *AE4115: Experimental Simulations Reader*, Delft University of Technology, 2021.

[6] Kerwin, J., Hadler, J., and Paulling, J., *The Principles of Naval Architecture Series, Propulsion*, The Society of Naval Architects and Marine Engineers, 2010.

[7] Phillips, W. F., and Snyder, D. O., "Modern Adaptation of Prandtl's Classic Lifting-Line Theory," *JOURNAL OF AIRCRAFT*, Vol. 37, No. 4, 2000.

[8] Bertin, J., and R.M.Cummings, *Aerodynamics for Engineers*, 5th ed., Pearson Education International, 2009.